
Crab Analysis and Comparison of RF and CNN method of Reconstruction

Rumman Neshat

18MS035

Under the Supervision of
Prof. Mosè Mariotti(UniPd, Italy)

Co-Supervision of
Dr. Rubén López Coto(IAA-CSIC, Spain)
Dr. Alessia Spolon(UniPD, Italy)

Thesis submitted to
Indian Institute of Science Education and Research, Kolkata

in partial fulfilment for the award of the degree of

Master of Science

in Physics



Department of Physics

DECLARATION

Date: 19/05/2023

I, Mr. Rumman Neshat Registration No. 18MS035 , a student of the Department of Physical Sciences of the BS-MS Programme of IISER Kolkata, hereby declare that this thesis is my own work and, to the best of my knowledge, it neither contains materials previously published or written by any other person, nor has it been submitted for any degree/diploma or any other academic award anywhere before. I have used the originality checking service to prevent inappropriate copying.

I hereby grant permission to IISER Kolkata to store the thesis in a database which can be accessed by others.

Signature



Name : Rumman Neshat

Department of Physical Sciences

Indian Institute of Science Education and Research Kolkata

Mohanpur 741246, West Bengal, India

CERTIFICATE

Date: 19/05/2023

This is to certify that the thesis titled " Crab Analysis and Comparison of RF and CNN method of Reconstruction " submitted by Mr. Rumman Neshat Registration No. 18MS035 dated 19/05/2023, a student of the Department of Physical Sciences of the BS-MS Programme of IISER Kolkata, is based upon his own research work under my supervision. I also certify, to the best of my knowledge, that neither the thesis nor any part of it has been submitted for any degree/diploma or any other academic award anywhere before. In my opinion, the thesis fulfils the requirement for the award of the degree of BS-MS.

Signature:

A handwritten signature in blue ink, consisting of a large, stylized 'M' followed by a series of loops and a long horizontal stroke extending to the right.

Name : Mosè Mariotti

Professor

Department of Physics and Astronomy

University Of Padova

ACKNOWLEDGEMENT

First and foremost, I would like to express my sincere gratitude to my supervisor, Prof. Mosè Mariotti, and my Co-Supervisor Dr. Alessia Spolon and Dr. Ruben Lopez Coto for their unwavering support, invaluable insights, and expert guidance throughout this research journey. Their patience, knowledge, and dedication have been instrumental in shaping this thesis and my growth as a researcher. I would like to thank Alessia for being available to clear my doubts in the MAGIC and for her valuable comments. I would like to thank Prof. Mosè Mariotti and Alessia for making my visit to the MAGIC group in Padova possible, where the interaction with the team helped me in improving my work.

I would like to express my deepest gratitude to other members of the MAGIC collaboration and, especially Davide Miceli, Ettore Marriotti, and Ivana Batković, whose constant help solved the problem I was facing.

I am deeply grateful to Prof. Tommaso Dorigo, and Prof. Sudip Garain for their stimulating discussion, valuable insights, and support that helped me in my research journey. My heartfelt thanks go to my parents, Md Neshat and Sayeeda Akhtari, my other family members Fauzia Neshat, Anzar Anis, Talha Neshat, Saima Neshat, and friends Shreyash, Harshal, Shashank, Madhur, Gopika, Calvin, Sourav, Praful, Narayan, Aashique, Adwait, Pranav, Amarjeet for their unwavering support, understanding, and encouragement throughout this arduous journey. Their belief in my abilities and unconditional love has been my constant motivation, providing me with the strength to persevere during challenging times.

ABSTRACT

The cosmic ray with the highest energies helps us to understand the composition and evolution of the universe. Because of the Magnetic field, it encounters on its way toward Earth, charged particle gets deflected; thus it's difficult to trace its origin. However, the Very High Energy gamma-ray photon being neutral doesn't get deflected and hence is used to study the source from where it is coming. In this thesis I have worked on the analysis of the Crab Nebula and Pulsar using both the MAGIC as well as Fermi-Lat Telescope. MAGIC being the ground-based telescope, could detect up to TeV Energies. With the introduction of Sum Trigger, it could also detect low-energy events up to 25 GeV. I have analyzed the Crab Pulsar using the Sum Trigger and produced the phasogram plot for it. I have also worked on the comparison of the reconstruction method by the MAGIC, which gives direction, energy, hadronness of the events. The two method that is compared uses Random Forest Machine Learning Algorithm and the Convolutional Neural Network(CNN) for reconstruction, respectively. For this, the analysis results for 20 hours of Crab Pulsar data is used. The other telescope that detects these VHE gamma-ray photons is Fermi-Lat which is space-based and measures from 20 MeV to 300 GeV only. I have analyzed the data from 2010-2018 to study the Crab Pulsar flux and to characterize the flares from the Crab Pulsar that were also observed in the years 2011 and 2007.

Contents

1	Introduction to VHE Astronomy	7
1.1	Introduction	7
1.2	Imaging Atmospheric Cherenkov Technique	8
1.3	Electromagnetic Shower	10
1.4	Hadronic Shower	10
1.5	Cherenkov Radiation	11
2	MAGIC Telescopes and Analysis	14
2.1	Signal Transfer in Magic	15
2.2	Trigger System	16
2.2.1	L0 Trigger	16
2.2.2	L1 Trigger	16
2.2.3	L3 Trigger	17
2.3	SUMTRIGGER	17
2.4	Image cleaning and Parameter	19
2.4.1	Hillas Parameters	20
2.4.2	Source Dependent parameters	20
2.4.3	Time Parameters	20
2.4.4	Directional Parameters	21
2.5	Stereo Image Parameter	21
2.6	Random Forest	23

2.7	Event Separation and Information Estimation	23
2.7.1	γ /Hadron Separation	24
2.7.2	Energy Estimation	24
2.7.3	Direction Reconstruction	25
2.8	Data Reconstruction	25
2.9	θ^2	26
2.10	Crab Nebula Analysis for 22/01/2022 and 31/01/2022	28
2.10.1	θ^2 Plot, Background Events	28
2.10.2	Spectral and Light Curve	30
2.11	SumTrigger Results for Crab Pulsar	32
2.12	Significance	34
2.13	Phasogram	35
3	An approach to compare CNN and RF reconstruction	37
3.1	Convolutional Neural Network	38
3.2	CNN MAGIC Analysis	39
3.3	Using Crab Pulsar for Comparison	41
3.3.1	Method :	41
3.4	Expected Plots	44
4	Fermi-Lat Analysis	46
4.1	Aperture Photometry	46
4.2	Unbinned Likelihood Analysis	48
4.3	Result and comparison	49
4.4	Light Curve Analysis(2010-2018)	50
5	CONCLUSIONS	54

Chapter 1

Introduction to VHE Astronomy

1.1 Introduction

The high-energy gamma-ray is produced by a mechanism like a pion decay, inverse Compton scattering in which the photons get scattered by the leptons and increases their energy, and Synchrotron radiation when the relativistic electron spirals in the magnetic field. Like the Synchrotron radiation, there is also curvature radiation but in this, the electron moves along the curved magnetic field hence producing the gamma-ray. The other process through which gamma rays are produced is called Electron Bremsstrahlung where the electron gets deflected in presence of the electric field and thus produces the gamma-ray photons.

The possible sources for very high energy γ ray photons or the cosmic rays are mainly Pulsars, Supernova Remnants, Binary stars, Active Galactic Nuclei, Gamma Ray Bursts, etc.

Out of all these sources, pulsars are one of the most interesting regions and heavily researched region. Pulsars are highly spinning neutron stars with intense magnetic fields which is formed due to magnetic flux and angular momentum conservation, when the star collapses.

The very high electric field generated due to neutron star in perpendicular to its magnetic field tears the surroundings producing e^+ , e^- . Hence filling it with plasma. The region around the Neutron star where we observed the close magnetic field lines are called magnetosphere (see fig.1.1) and the region beyond that is called as Pulsar wind region. Because of the curvature radiation, in the slot gap γ ray photons are produced. These photons achieves very high energy due to inverse Compton scattering because of leptons present in the Neutron star outer gap region (see fig 1.2). We can detect this *gamma* and the VHE(Very High energy) particles in order to get the physics of the region from which it is coming. In the coming section, it is described in detail way to detect these VHE particles or cosmic rays and get meaning out of them with a particular focus on the Crab nebula which is energized by the Pulsar.

1.2 Imaging Atmospheric Cherenkov Technique

There are two methods to detect high-energy photons or particles from different Galactic and Extragalactic sources. One is to use the satellites directly detecting the photons out in space, but due to its small collection area, there is a certain energy range up to which only it is effective. Another way is to have a ground-based telescope like that of MAGIC(Major Atmospheric Gamma Imaging Cherenkov Telescopes) in order to detect high-energy photons up to Tev. However directly, these photon cant be detected as it interacts with the air molecules present in the atmosphere. Thus these VHE photons produce an EM cascade or atmospheric shower. These showers can be categorized into two types:

- i) EM shower
- ii) Hadronic Shower

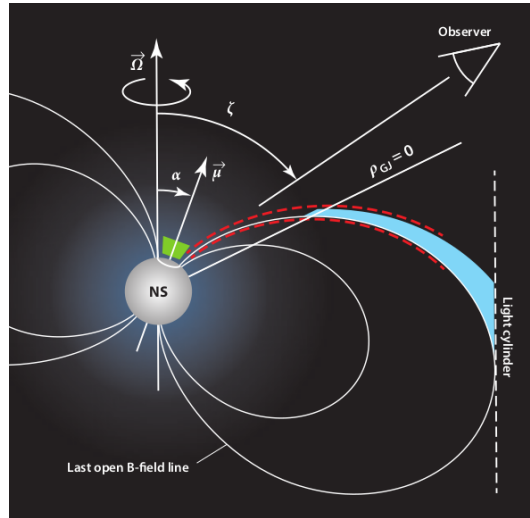


Figure 1.1: Neutron star magnetosphere. Credits [1]

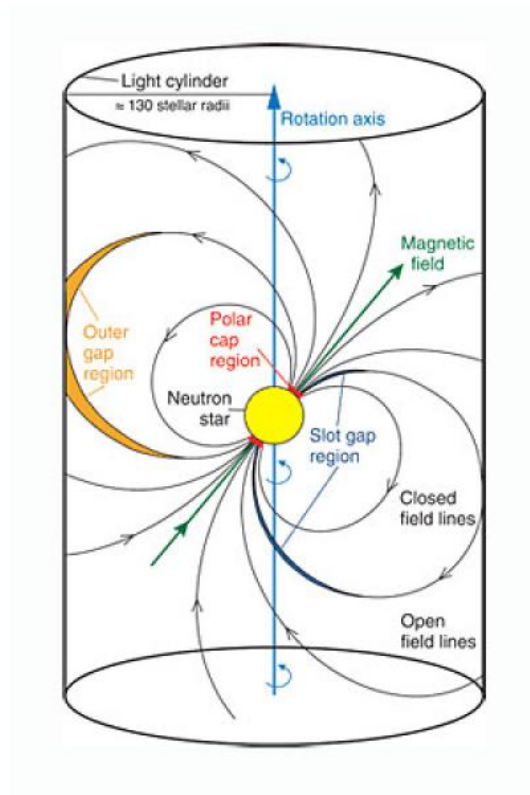


Figure 1.2: Model for Pulsar Gamma Ray emission. Credit MAGIC Collaboration.

1.3 Electromagnetic Shower

When a photon with energy greater than 20 MeV enters the Earth’s atmosphere, it produces e^+ and e^- in the presence of the nucleus of air molecules. These e^+ , e^- produces photons due to bremsstrahlung process. The photons produced are still very energetic thus producing e^+ , e^- and the photons. In this way, an EM(Electromagnetic) shower or cascade is produced. When the energy of e^+ , e^- being produced in the cascade reaches below the critical energy E_c , which is the threshold for the production of the photons, the shower further development eventually stops. The height from the ground at which it stops is called Shower Maximum, H_{Max} which is inversely proportional to the log of energy of the gamma-ray.

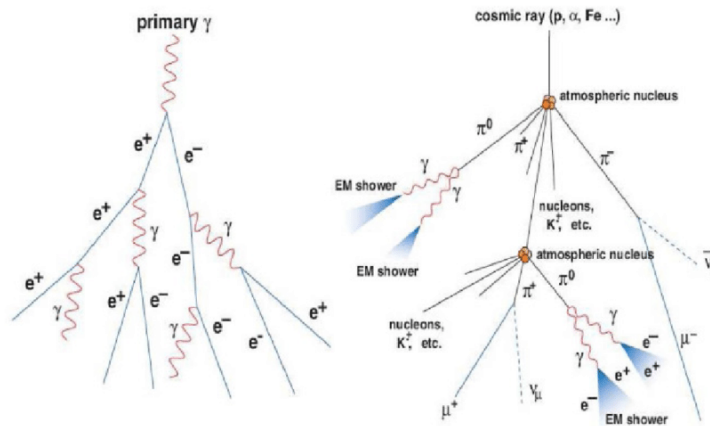


Figure 1.3: schematic view of γ and hadronic shower. Image is taken from [2]

1.4 Hadronic Shower

When the high energy hadron interacts with the atmospheric nucleus via strong interaction, the particles being produced in abundance is the pion. The hadrons and pions undergo further collision, once the energy of particles reaches the threshold energy i.e energy required for further production, the shower stops. The neutral pion produced in the cascade also decays into photons. These photons form the sub Elec-

tromagnetic cascades.

The hadronic shower developed more laterally as compared to the gamma ray photons producing EM shower. Because of the strong interaction, the transverse momentum of hadrons produced is higher as compared to that of leptons like e^+ , e^- in the EM shower. Due to this, the average time dispersion for EM shower is very less than compared to the hadronic shower. Furthermore, the development of the shower is more symmetrical in the case of EM whereas the hadronic shower is an irregular kind with composed of several EM sub shower mostly caused due to decay of π^0 to $\gamma\gamma$, is shown in the figure 1.4.

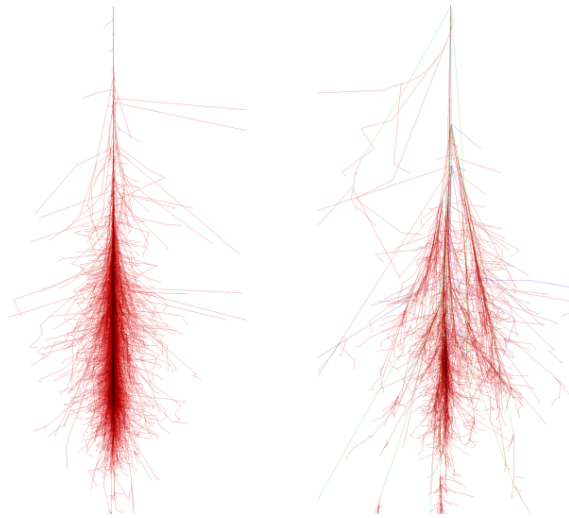


Figure 1.4: Simulation showing the development of γ and hadronic shower. Credits [3]

1.5 Cherenkov Radiation

Several of the particles that originated in the cascade are relativistic i.e in the propagation medium their speed exceeds the speed of light. Hence when these particles travel in the atmospheric medium, they polarizes it. When the speed v of these ultrarelativistic charged particles is greater than the speed of light in the medium of

Refractive Index n , the induced polarization is not symmetric 1.5. To compensate for this effect the Cherenkov radiation is produced. The radiation emitted is in form of a cone 1.7 whose angle is given by :

$$\cos\theta = \frac{c}{vn(\lambda)} \quad (1.1)$$

Here $n(\lambda)$ is the spectral index of the medium. The maximum angle θ derived from the above equation is $\lesssim 1$.

In the case of γ shower, its energy is directly proportional to the Cherenkov density detected at the ground. The Cherenkov radiation thus produced is detected on the ground and is used to convert the meaningful information from the shower to the data. The purpose of this imaging technique is to separate the γ and hadron-initiated shower, direction reconstruction, and energy estimation.

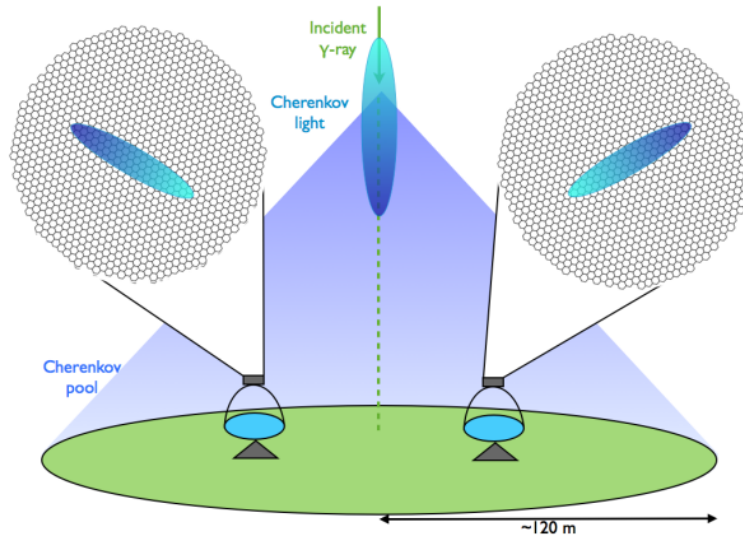


Figure 1.5: View of Cherenkov radiation being detected by the MAGIC telescope [3]

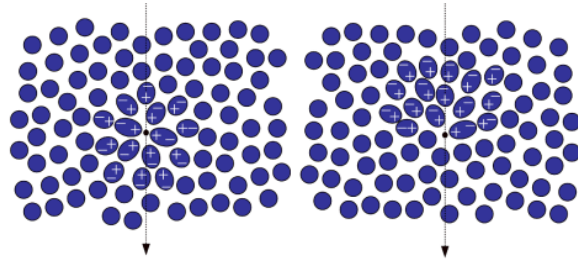


Figure 1.6: When $v < \frac{c}{n}$
polarization induced is symmetrical and when it's $> \frac{c}{n}$, unsymmetrical polarization
[3]

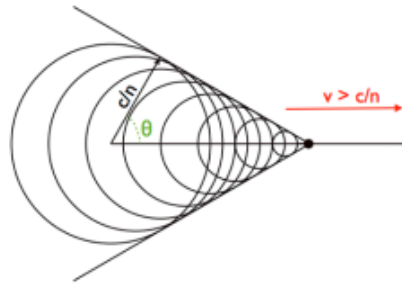


Figure 1.7: Emission of Cherenkov cone[3]

Chapter 2

MAGIC Telescopes and Analysis

MAGIC (Major Atmospheric Gamma Imaging Cherenkov Telescopes) is a large-sized ground based telescope constructed at La Palma Island, Spain, in order to achieve the task of converting the Cherenkov radiation to some meaningful information. The energy range in which it could operate is 100 GeV-100 TeV and with sum trigger it could detect events happening at 25 GeV. Its effective area is $10^5 m^2$. It is equipped with large parabolic reflectors which collect the maximum amount of Cherenkov light and pixelized cameras at the focus of the mirror with a fast response.

The electric signal is sampled and digitized for each pixel when a trigger occurs. Data Analysis for the MAGIC output is done by the software called MARS (MAGIC Analysis and Reconstruction Software). It converts the ADC (Analog to digital Converter) counts to a number of photoelectrons (phe) corresponding to each pixel. The purpose of this software is to reconstruct the events generating the shower, and estimate its energy and direction.

The signal recorded is converted to counts corresponding to each pixel. This raw data with output in counts vs time is converted to root format using a program called merpp (MERging and Preprocessing Program). After this the ADC counts is

converted to photoelectrons using a program called Sorcerer (Simple, Outright Raw Calibration; Easy, Reliable Extraction Routines). Once this is done, now we need only relevant pixels of an event corresponding to an event which we will discuss in detail in the coming section.

2.1 Signal Transfer in Magic

In this section, I have briefly described how the MAGIC telescope stores the signal and converts them to meaningful information. The Cherenkov lights, after being reflected from the reflective parabolic mirrors of MAGIC, are detected by the camera located in the focus of the MAGIC mirror. The camera is composed of the Photo Multipliers Tube (PMT). In its entrance the Cherenkov photons are converted to photoelectron and later in the dynodes it is multiplied to reach a charge that could be detected electronically above noise. The readout system then processes this electrical signal. The PMT is supported by the hexagonal shape Winston cone, which focuses the light on the PMT window and also prevents the light from entering from a large angle to the PMT, which could be from the night sky background or the light that is reaching after being reflected from the ground, thus making the system more efficient. The PMTs present are grouped into 169 clusters of seven pixels each. These electrical signals from each pixel are again converted to analog optical signals which are passed through optical fibers to the counting-house, where with the help of photodiodes it is again converted to electrical signal for further reading. In the counting house, the electrical signals are divided into two parts, one part is stored in the DRS4 chip and the other one is sent to the triggers system(L0 trigger, L1 trigger, Sum Trigger, L3 trigger), when the result from the L3 trigger is positive, the signal stored in the DRS4 chip is sent to the Data Acquisition, after being converted to digital from analog to digital converter. In the next step, I will explain briefly about the trigger system and in detail about the sum trigger as the major part of analysis done in this thesis are

of sum trigger data.

2.2 Trigger System

In this section, I will illustrate the trigger system responsible for storing or discarding the events. The trigger system is designed in such a way that helps to discriminate the signal i.e., the Cherenkov events, from that of noise or the night sky background(NSB). Below explained is the three trigger level [4] :

2.2.1 L0 Trigger

This trigger passes on the analog signal received from the PMT to next level trigger if the pulses received are above a certain threshold mainly called as discriminator threshold(DT). The threshold value are determined at the beginning of data taking based on moonlight available or the background noise. Low moonlight means the DT will be low, high moonlight means the DT will be more. The point to be noted here is that L0 trigger corresponds to each pixel PMT and how it is different from the other trigger method that is the sum trigger will be explained in the later section.

2.2.2 L1 Trigger

The signals received by the L0 trigger act as input to the L1 trigger. In this trigger level, the camera pixels are divided into 19 macrocells, with one layer of hexagonal cells overlapping with the other in all cases, as you can see in the image below. This trigger is used to identify the next neighbor pattern, which is helpful to find the spatial relation between the pixels. As explained above, the showers produce a compact disc-like or elliptical shape on the camera so the isolated pixels points, which may be the noise, could be removed in this trigger level. In the standard mode, a 3NN (next neighbour) pattern is used, so the pixel having three next neighbors is kept; otherwise, it's discarded.

2.2.3 L3 Trigger

The L3 trigger is used for the stereo observation i.e., to observe whether the event detected by both the telescopes are same or not. If both telescopes in the given time window record an event, then the L3 trigger level would be positive. The time gate value for this trigger is around 180 ns. Once corrected for the geometrical orientation of the two telescope, if the signal from the input level of L3 trigger is within 120ns then the signal is readout.

2.3 SUMTRIGGER

With the normal trigger system, the low energy gamma ray events happening in our universe, like that of pulsars, gamma-ray bursts, etc, are difficult to detect. Hence with this new trigger system, events as low as 25 GeV could also be detected.

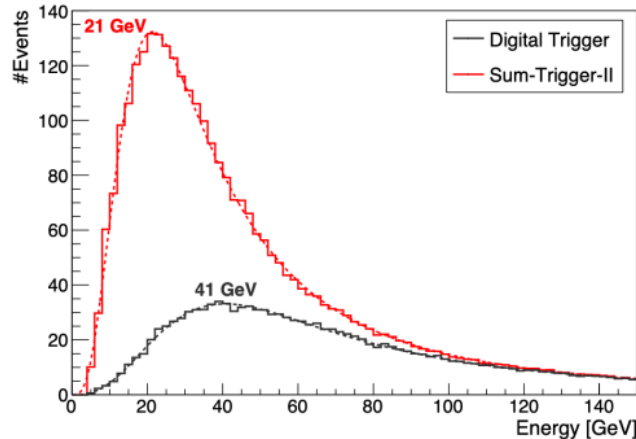


Figure 2.1: Illustration of Performance of sum Trigger II and Digital Trigger. It can be seen with Sum Trigger II the high performance around 21 GeV is Observed. Credits[5]

The MAGIC camera pixels are divided into 55 macrocells in three layers (see fig 2.2), with all three layers overlapping partly. The patches are optimized in such a

way that every pixel in a macrocell is taken into account for the data reading process. This method is quite useful as those pixels which are discarded in the standard trigger, due to their pulses below the discriminator threshold or those pixels which do not survive the L1 trigger but could contribute to deciding the result of the event, are also taken into account.

In these macrocells each one contains 19 pixels each and total 529 pixels lie in these combined macrocells. Here unlike L0 trigger system, the signals from each pixel in a macrocell are added analogically and then the result is passed to the discriminator. In the figure 2.1, where the minimum energy threshold upto which these two trigger system works better are shown for comparison. The performance for sum trigger II stereo events are better at low energies. The low energy γ ray events produce low photon density, hence to capture these it is necessary to sum all the analog signals where gamma ray image is scattered. In standard trigger, the low photon density or signals concentrated in small region, reduces its performance which is resolved in the sum trigger to observe low energy events. In the image 2.2, proper schematics of sum trigger is given, to understand this process. For more information [6] [7].

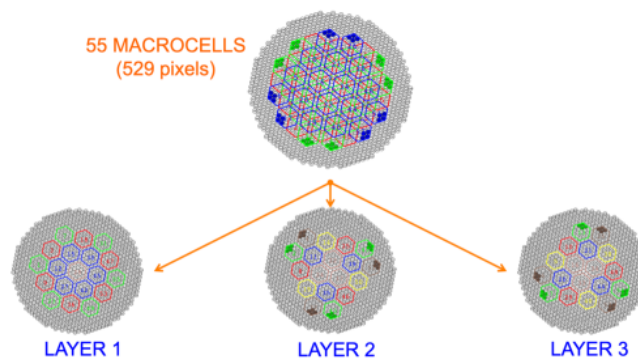


Figure 2.2: Depiction of design of Sum Trigger camera pixel where it is divided into three layers and with overlapping macrocells. Image Credits [5]

2.4 Image cleaning and Parameter

In this stage, only relevant pixels of the camera is kept and the rest are cleaned. Parameters important for energy estimation, direction reconstruction, and γ and hadron separation are calculated. The program responsible for this is called star.

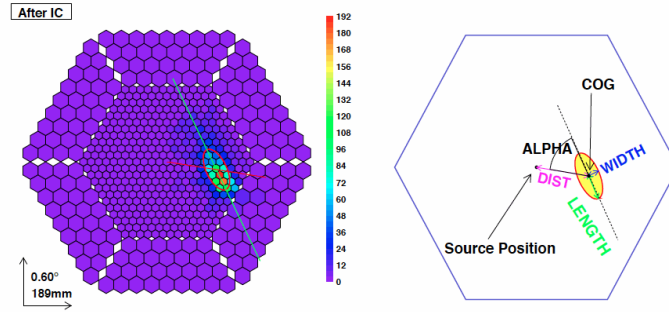


Figure 2.3: Figure showing image cleaning and image parameters. Image is taken from MAGIC wikipedia.

Those pixels which are useful to give information about the shower are kept in this step. Each Pixel has value in terms of the charge i.e the number of photoelectrons and the arrival time of the radiation. In this method a pixel is termed as core pixel if its phe values is above the certain threshold value Q_c , the arrival time should not differ from the mean arrival time of the core of the image by Δt_c , and it should be adjacent to another core pixel. For the boundary pixels the thresholds changes to Q_b , Δt_b . The rest of the pixels are cleaned. Once this is done, the values are stored in the data. In order to calculate the parameters the resulting image is fitted with an ellipse as shown in the figure. As since we are interested in VHE γ ray, the shower generated is more symmetric, compact. The projection of these shower will be compact and elliptical on the ground, hence the resulting image observed on the camera is elliptical.

2.4.1 Hillas Parameters

Size: The total number of phe in the image is calculated, which is important to estimate the energy of the primary γ as the higher the energy more the Cherenkov density, hence more is the size.

Width: It is the RMS length along the minor axis of the fitted ellipse which is important to know the lateral development of the shower.

Length: It is the RMS spread along the major axis of the ellipse in order to measure the longitudinal development of the shower.

Centre Of Gravity(COG): It is computed as the mean of X and Y along the camera coordinates.

Conc(N): In order to know about the compactness of the shower, this parameter is calculated, which measures what fraction of the image resides in the N brightest pixels. For Hillas parameters see [8].

2.4.2 Source Dependent parameters

Dist: Angular distance from the COG to the expected source position in the camera.

Alpha: Angle between the major axis of the ellipse and line connecting COG to the expected source position. This angle should be small for the γ like showers.

2.4.3 Time Parameters

Time(RMS): The arrival time of hadron-like and gamma-like showers is very different. This factor is important to differentiate between the two showers. It is the RMS of the arrival of the pixels that survived after cleaning. For γ like events, it will be low as compared to hadron-like events.

Time(Gradient): It is the slope of the linear fit of the arrival time along the major axis of the ellipse in order to know about the directional development of the shower.

Image Quality Parameters

The image contained in the camera could be very noisy, hence to evaluate this **Leakage**(Fraction of Source image contained in N outermost rings) and **Number Of Islands**(no. of non-connected pixels that survived the image cleaning) is calculated.

2.4.4 Directional Parameters

This is used in order to differentiate between the head and tail of the shower. In general, most of the charge is concentrated in the head. For this **Asymmetry**(distance between showers COG and highest charge pixel) and **M3Long**(Third moment of shower image along major axis) is calculated.

Running star(programme in a standard MAGIC software) would also separate data based on the quality i.e. whether it is bad or good, as its a significant probability that our event might capture noise due to different weather conditions or other factors. Once this is done, the data from the two telescopes are merged via the program called superstar, and other parameters are calculated.

2.5 Stereo Image Parameter

To reconstruct the three-dimensional development of the shower, the data from two MAGIC telescopes are merged. This is done by running a program called superstar.

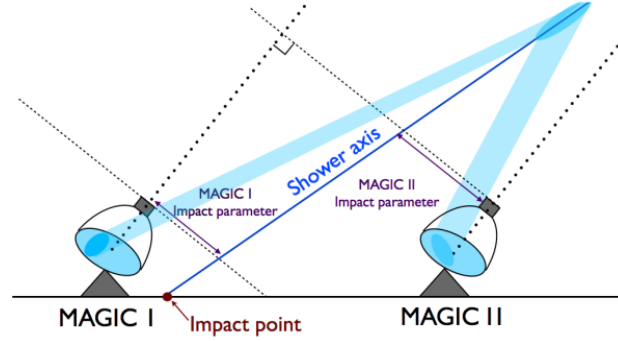


Figure 2.4: Stereo Image Parameter finding [3]

Impact Point: As shown in the figure 2.4 when the ellipse from two telescopes is superimposed along its major axis, then the point on the ground along the superimposed ellipse is the impact point.

Shower axis: The crossing point of two major axes of two ellipses from two telescopes in the camera plane.

Height of Shower Maximum: Using the shower axis and the angle with COG of the ellipse from two telescopes are used to estimate the energy and helps in γ and hadron separation. As for the hadron, lateral development of the shower is more and hence more the H_{Max} .

Cherenkov Radius: Radius of the Cherenkov pool at the height of Shower maximum.

Cherenkov Photon Density: Cherenkov photon density at the Height of Shower Maximum.

To estimate the energy, direction reconstruction, and γ /hadron separation, we use a machine learning algorithm called Random Forest. In the coming section, Random Forest is described in brief, and then we went on to discuss how it is used in our analysis.

2.6 Random Forest

It is the supervised machine learning method to split data continuously based on certain parameters. The idea is to construct the decision tree based on the feature which able to classify the data easily and more better.

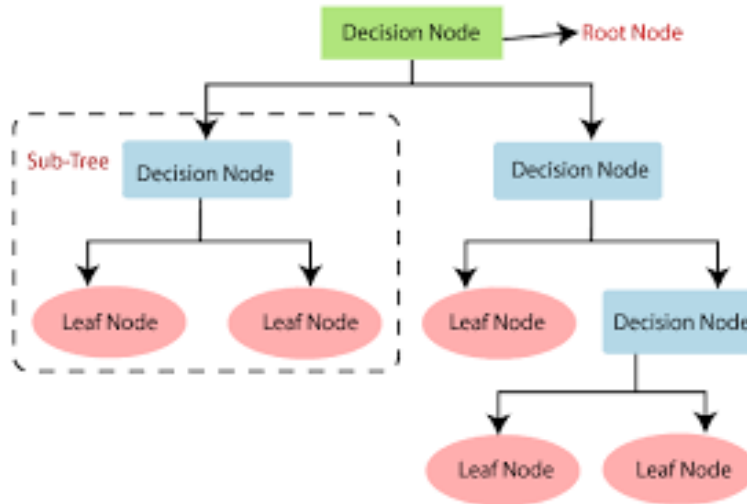


Figure 2.5: Decision Tree

The nodes are selected such that the feature or the parameter there gives the highest information gain regarding the data. Once the parameter of the root node is selected, it is divided based on the attributes of the parameter, and then the further branch node is selected in the same way. The figure 2.5 depicts the construction of the decision tree.

2.7 Event Separation and Information Estimation

As described earlier, Random Forest is used to estimate energy, γ /hadron separation, and energy estimation. For this, our RF is needed to be trained. The MC(Monte Carlo) simulations are performed in the same conditions, and the data corresponding to this is available so that we can train the RF.

2.7.1 γ /Hadron Separation

The MC samples are split into Test and Train. The Train data is used to train the RF about the γ like events whereas the off data (taken at the same zd (Zenith distance) condition but with no source) is used to train RF (Random Forest) about how the hadronic events would be like. The Algorithm constructs the decision trees based on the parameters. As described above nodes parameters are decided on the basis of information gain or minimizing the Gini index. The Gini index for this is given by: For more information see [3]

$$Q_{Gini} = 4 \frac{N_\gamma N_H}{NN} \quad (2.1)$$

where N_γ is the γ like events and N_H is the hadron events, and N is the total events. The RF is trained by running a program called as coach. Once RF is trained, the ON(data that needed to be characterized) is classified using the program called melibea. The event is then assigned hadronness based on the formula :

$$h = \sum \frac{h_i}{n}$$

where h_i is the hadronness on the i^{th} branch and h is the final hadronness. The event is assigned hadronness 0 if it is γ like or 1 if it is hadron-like.

2.7.2 Energy Estimation

To estimate the energy the RF is trained by minimizing the variance of E_{True} , which is calculated as:

$$E_{bias} = \frac{E_{est} - E_{True}}{E_{True}}$$

where E_{est} is calculated as the average of the RMS of energy from both the telescopes in each bin. The binning is done w.r.t parameters such as size, cherenkov radius. This could also be used to determine the energy threshold of the telescope.

2.7.3 Direction Reconstruction

It can be done by the crossing method introduced in the stereo observation. However, for single-using Disp it could also be done. The disp is given by the distance between the source position of gamma-ray and the COG:

$$disp = A(size) + B(size) \frac{width}{length + n(size)leakage}$$

where A and B are second-order polynomials of log(size)

2.8 Data Reconstruction

As shown in the figure 2.6, the data reconstruction is divided into three parts : low level data reconstruction, intermediate level data reconstruction and the high level data reconstruction.

Low Level Data Reconstruction: This process is done on the site, where raw data is converted to meaningful information. merpp(Conversion of data to root file), sorcerer(The calibration of the signal), star(image cleaning and calculation of parameters) are done on the site. These readable data then are used by the analyzers.

Intermediate level data reconstruction : After obtaining the events and the necessary parameters, we need to merge the data from the two telescope (superstar), train the random forest(coach).The Random forest is trained with the MC(monte carlo simulation) and the off data(data taken to understand the background) and get our results through melibea in the MARS software. In the following section I have talked in detail about how we reach to the conclusion of hadronness, energy reconstruction, direction reconstruction.

High Level Reconstruction : In this final stage, we use the result to obtain the light curve, spectrum, skymaps. The method called flute(light curve, spectrum), odie(to calculate significance), caspar(to have skymaps) are used to obtain respective results.

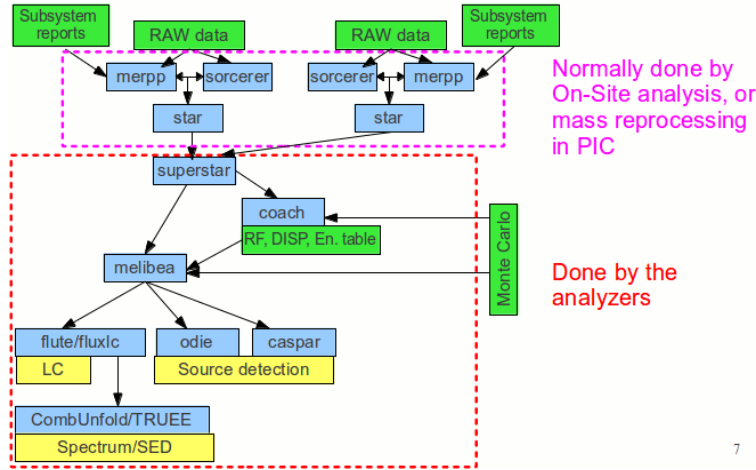


Figure 2.6: Overall view of data analysis scheme in MAGIC. Credits MAGIC wikipedia.

2.9 θ^2

Through our analysis, we use the obtained results of hadronness, energy, direction to apply cuts to our data to know whether the events in the data sample contain a signal. One of the cuts that are applied to capture the signal is called θ^2 , which is calculated by the Odie program in Mars software. θ is the angular distance between the reconstructed position of the event and the true source position. The schematics to calculate θ are shown in the figure 2.7.

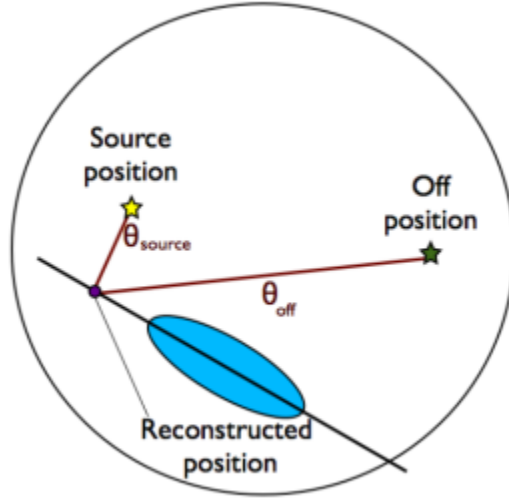


Figure 2.7: Illustration of θ_{on} and θ_{off} credits [3]

The events which survive all the cuts from our analysis, like θ^2 , energy, hadronness, etc are said to belong to the signal and used to fill the signal histogram. The events also contains those that are not induced due to γ and by hadrons or e^+, e^- etc. These events are called as off events or the background and in the signal histogram it is also plotted. The θ_{off} is the angular distance for these off events between the off position and reconstructed position. The number of excess events is defined as:

$$N_{excess} = N_{on} - \alpha \times N_{off}$$

Here α is the ratio between the length of ON and OFF region. This is helpful in determining the significance which is explained in later parts.

2.10 Crab Nebula Analysis for 22/01/2022 and 31/01/2022

After Melibea is done, we have information on whose basis we could extract the signal i.e data in which we are interested. Since I wanted to analyze the data from Crab nebula I gave the following cut:

Zenith Distance = 5 - 35 ,

Hadronness cut: 0.8, Since we are considering crab nebula therefore we get contribution from a lot of charged particles coming from the wind zone.

theta2 cut < 0.02

After this, we apply the flute program with the following cut in order to get information like Energy Spectrum, Light Curve, etc.

2.10.1 θ^2 Plot, Background Events

To have an idea of the number of hadronic events in the signal region, we have the θ^2 plot. The number of events inside the signal region is called N_{ON} , the events that are not of our interest are called N_{excess} . The point to be noted here is N_{off} and N_{excess} are different.

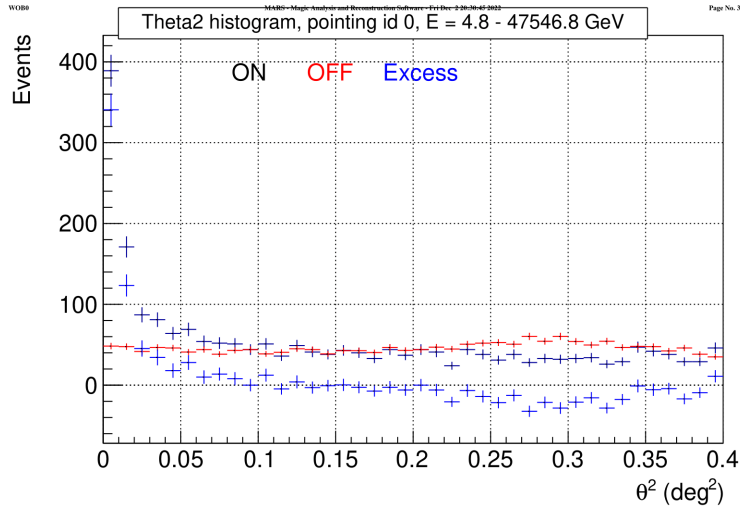


Figure 2.8: θ^2 Plot

The figure 2.8 is the θ^2 plot obtained for the Crab Nebula Analysis. One thing to notice here is the peaking of on events near the center or the source position. The background or the off events remains flat throughout. Implying most of the events triggered in our signal are coming from the source.

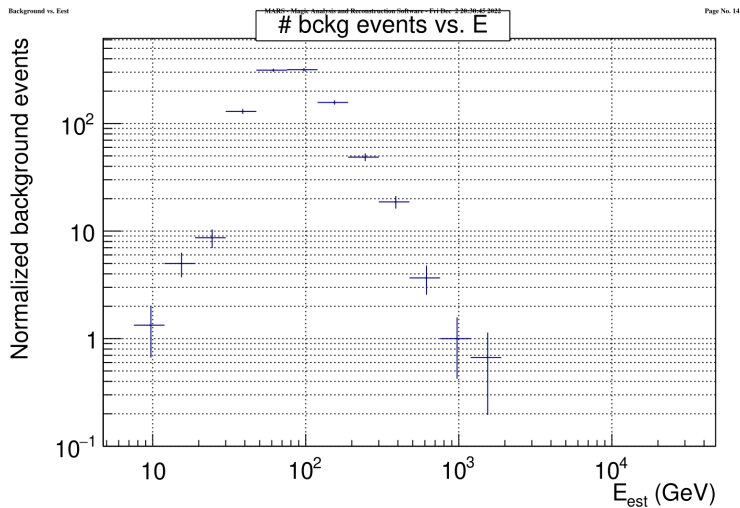


Figure 2.9: Normalized back ground events vs Energy

The plot 2.9 shows the normalized number of background events at different energy ranges.

2.10.2 Spectral and Light Curve

The γ ray differential spectrum is given by no. of photons per unit time per unit energy per unit area.

$$\frac{d\phi}{dE} = \frac{dN_{\gamma}(E)}{dEdAdt}$$

The program called flute takes the input as the melibea data. The number of gamma events is given by the N_{excess} .

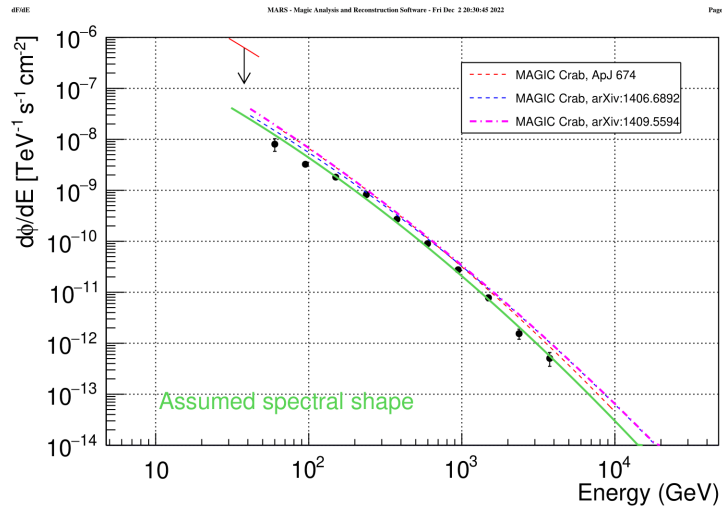


Figure 2.10: Energy Spectrum : $\frac{d\phi}{dE}$

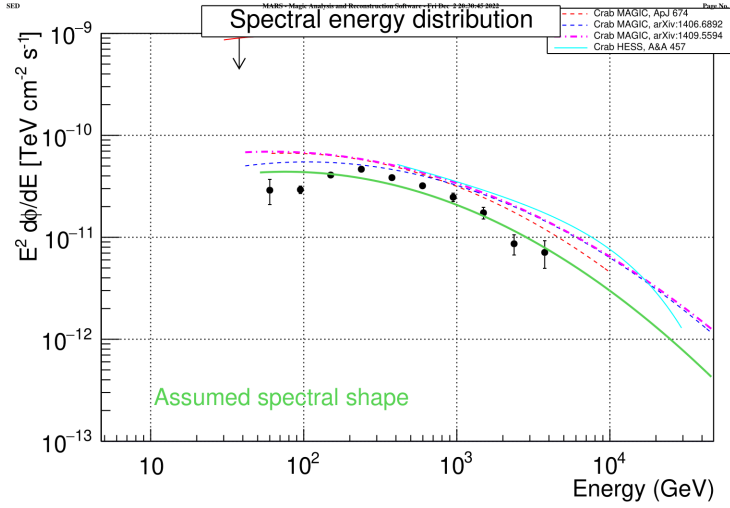


Figure 2.11: $E^2 \frac{d\phi}{dE}$

The light curve shown in the figure 2.12 is taken as the integral of $\frac{d\phi}{dE}$ over a given time range, integral over the given energy. For the analysis done here, the light curve is plotted by night wise for both the γ events and the background events.

$$\phi = \int \frac{d\phi}{dE}$$

For the next part, we will extend this analysis to Pulsars using the sum trigger data.

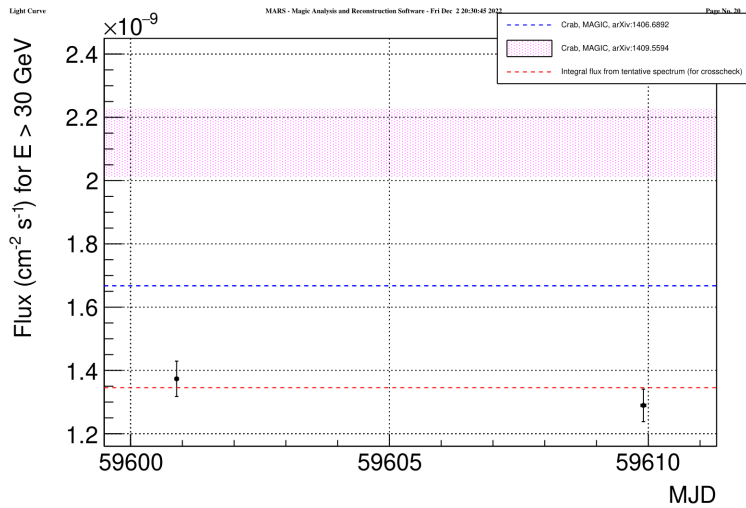


Figure 2.12: Light curve for crab nebula corresponding to night wise binning

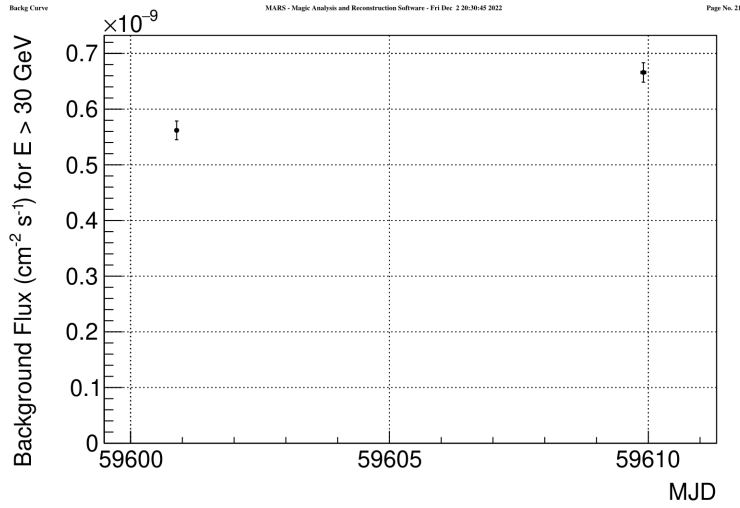


Figure 2.13: Light curve for background corresponding to night wise binning

2.11 SumTrigger Results for Crab Pulsar

With the standard trigger system, while observing the crab pulsar no signal was obtained. Hence the sum trigger is quite important to detect low energy events. Below are the results shown for the data analysed using the Sum trigger data for an effective 6.4 hours.

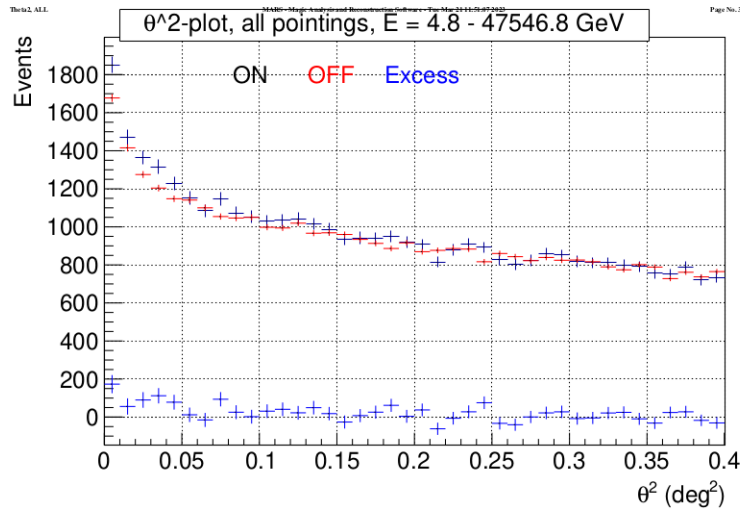


Figure 2.14: θ^2 Plot obtained for Crab Pulsar

The θ^2 plot obtained here is quite different as compared to that of Crab Nebula. The on and off events obtained here is defined depending on its arrival time with respect to the pulsar time phase. To give reference, the on events belong to the peaks plotted in the light gray area of phasogram (see fig 2.17) and off events are the background which is also shown in phasogram in dashed gray area in the figure 2.17. In the figure 2.14 we can see both on and off are peaking near the center. This strange result is observed in case of Crab Pulsar because of the fact that the Crab Nebula acts as the background for the Crab Pulsar. And therefore we observe both on and off peaking near the center because of their same position.

Spectral Energy Distribution for Crab Pulsar:

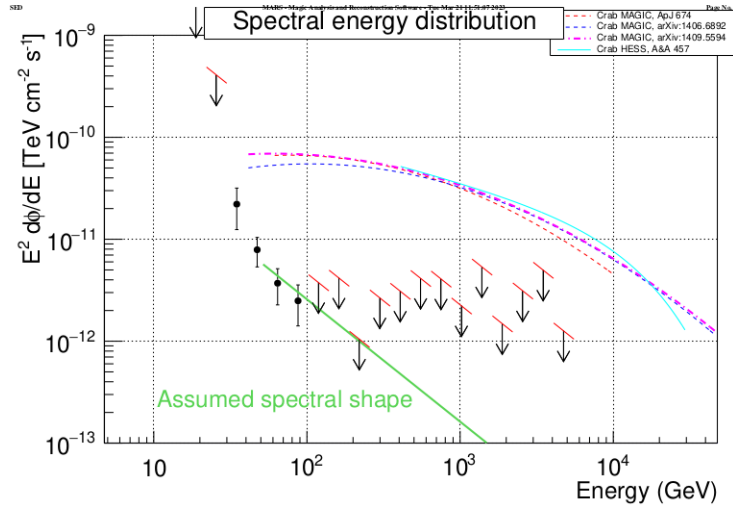


Figure 2.15: SED for Crab Pulsar

Fig : In the $E^2 \frac{d\phi}{dE}$ curve for Crab Pulsar it could be seen I am able to obtain signals which I was not able in case of Standard trigger.

Flux:

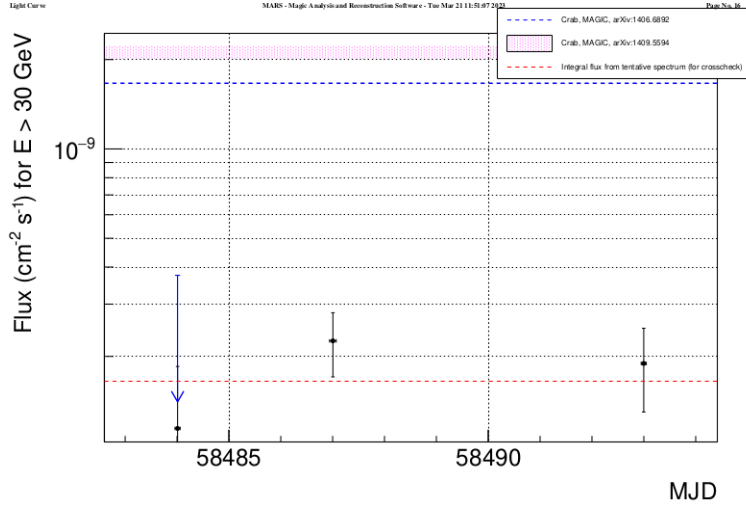


Figure 2.16: Flux Plot obtained for Crab Pulsar

2.12 Significance

Once we have obtained the N_{excess} from our analysis, we could calculate the statistical significance of the signal in order to know whether we are getting signal from the region or not. The VHE astronomy uses the Likelihood hypothesis, to understand whether the source is detected or not. The significance based on this is given by LiMa [9] as :

$$\sigma_{LiMa} = \sqrt{2(N_{on} \ln[\frac{1+\alpha}{\alpha} \frac{N_{on}}{N_{on}-N_{off}}] + N_{off} \ln[(1+\alpha) \frac{N_{off}}{N_{on}-N_{off}}])}$$

Upon the gaussian approximation, this could be given as:

$$\sigma \frac{N_{ex}}{\sqrt{N_{off}}} = \frac{N_{excess}}{\sqrt{N_{off}}}$$

If the significance is above 5σ over the background, the detection of source is confirmed.

2.13 Phasogram

For the Pulsars, the histogrammic representation of its phases(arrival time of events from the pulsar) is done through phasogram. The analysis involving this is called as phasogram analysis. In MAGIC the phases are obtained on the signal events using the ephemeris of the time period in which pulsar is analyzed through Tempo2 software. This computes the phase based on the arrival time of events, and add it in additional column in the root file corresponding to each event. We expect the observation of peak and then the background in periodic manner for the pulsar because of excess emission along the open magnetic field lines of the pulsar. With the analysis of Sum Trigger data, I have obtained the phasogram with the significance of 5.1σ . The point to be noted here is that all the result which we have got is after applying the cuts which we got from the analysis on the events. The number of on and off events are found based on the phase mentioned in [7], given in table below:

Phase(ϕ)	
0.0 - 0.026	N_{on}
0.377-0.422	N_{on}
0.983-1.00	N_{on}
0.520 - 0.870	N_{off}

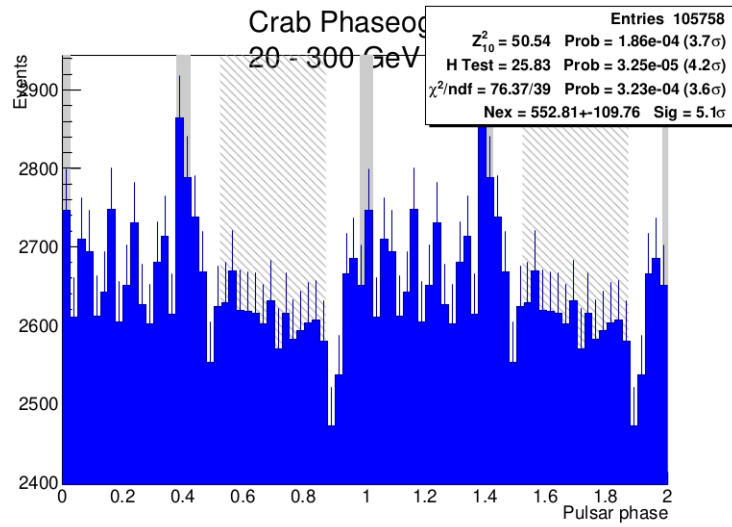


Figure 2.17: Phasogram for the Crab Pulsar obtained using the MAGIC Analysis

The Phasogram analysis for the Crab Pulsar have been used later for the comparison of the reconstruction method.

Chapter 3

An approach to compare CNN and RF reconstruction

In this section, I tried to compare the two methods of reconstruction i.e. through the random forest machine learning algorithm and through the convolutional neural network(CNN) deep learning algorithm. In the random forest reconstruction method, some of information are lost during the cleaning of the calibrated image. This lost information can be important as it could help predict the hadronness, energy, direction to more certainty. The CNN algorithm, specially designed to characterize and recognize patterns, is expected to give comparable or better results as compared to RF because we are giving input as the calibrated image directly. In the coming section, I will briefly describe CNN, explain the reconstruction method, and will compare the two algorithms. I will also briefly describe the source we are using for this comparison.

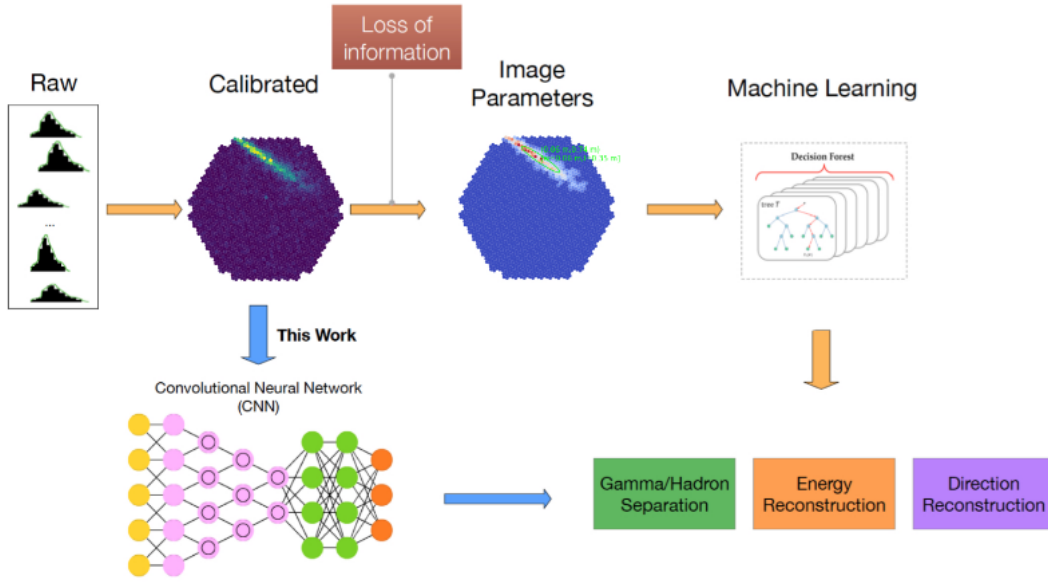


Figure 3.1: In the random forest reconstruction method, the calibrated image is cleaned first of all causing loss of information, and then the parameters determined is feed to ML algorithm. However in CNN the calibrated image itself is given as input and hence we expect more precise analysis. Image credits to [10].

3.1 Convolutional Neural Network

The CNN(convolutional neural network) is the supervised deep learning algorithm used to identify patterns or recognize images. The CNN’s neural network is designed in such a way that it takes the array data as input and performs the operation on them. The image visualised as a pixels of 3D array, Sound as 2D array etc can be given as input, and with the help of trained algorithm could be recognized.

The convolutional neural network is inspired by the networks of neuron and its capability of passing information and responding towards the stimuli. The CNN is made of deep hidden layers consisting alternating convolutional and pooling layers. The convolutional layer takes the 3d matrices as input through the input layer performs the dot product with it and the result is then used as input for the next layer.

The pooling layer on the other hand merge the features that are same.

In the figure 3.2 , the diagrammatic view of how CNN works is shown. One of the convolutional layers will recognize the corners or edges, with that as input the other will recognize the shapes and in the same way it will go, the trained algorithm will finally give the output. The more deep the neural network is, the more reflection of properties of data in the result will be.

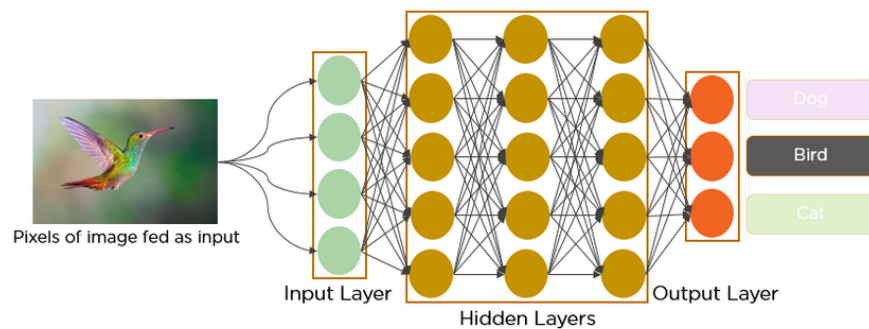


Figure 3.2: In the figure above it is shown how the CNN works, the image in form of 3D array is given as input and the operations are performed by the Convolutional and pooling layer, finally we get the output.

3.2 CNN MAGIC Analysis

The reconstruction work by CNN is performed by ([11]). The Analysis includes the Separation of hadronic and γ events(binary classification Problem) , Energy Reconstruction of the events recorded(single output regression), Direction reconstruction(double output regression). The novel analysis method designed by ([11]) includes the proposal of TSE(Transfer Snapshot Ensemble) for the energy reconstruction which saw an improvement by 30% and Simplicionet(put reference) model was built for the separation of γ and hadronic events.

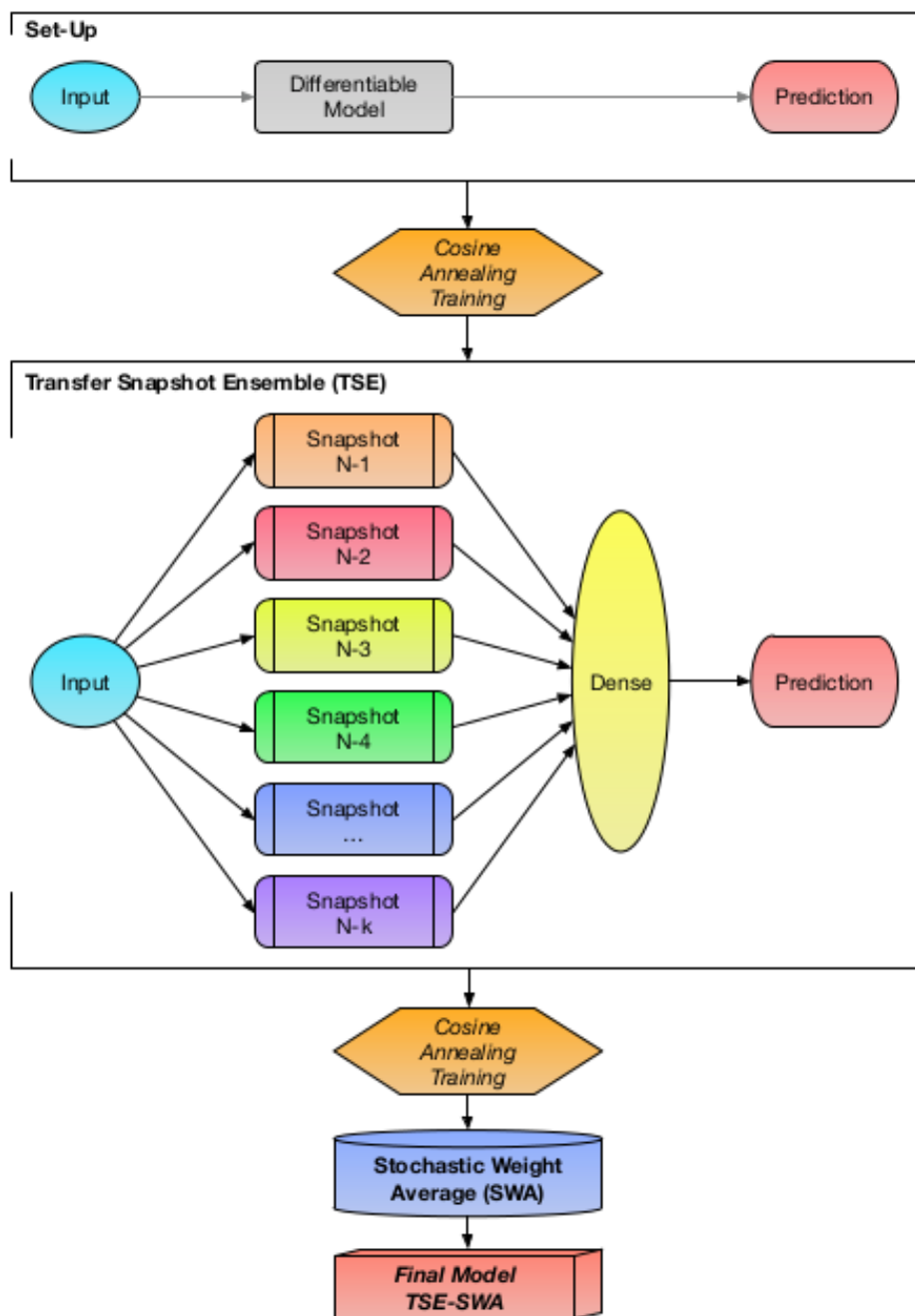


Figure 3.3: Depiction of TES-SWA work used in reconstruction. Credits to [11]

3.3 Using Crab Pulsar for Comparison

The next part of this thesis is focused on the comparison of two methods of reconstruction. One is CNN whose reconstruction is shown previously and the other is RF which we use in the MAGIC till now. For the comparison we have used the events obtained by observing the Crab Pulsar. The analysis that is done using CNN is source dependent, so while obtaining the parameters like that of θ^2 and applying cuts to calculate the significance, the result will be biased towards CNN as in RF source independent analysis is done. To get rid of this problem, we used the phase analysis from the events of Crab Pulsar. In the Phase analysis we expect this problem to solve as it depends on the arrival time of events and biasness to resolve. Crab Pulsar being a Galactic source is hence used. In the coming future work, we will be trying to compare CNN and RF to other more sources too. Earlier we have checked this performance with Markarian.

3.3.1 Method :

The Crab Pulsar data corresponding to 20 hours was taken and was analysed using both the methods. Since the root file cannot be used directly for CNN Analysis, therefore it has to be converted to HDF5 file format. After analysing the Crab pulsar with both the RF and CNN methods the results like energy, direction, hadronness etc for all the events are stored in a tabulated form along with the Run Id, Event Id and timestamp for each event so that they could be compared easily. For the comparison the idea is to mix the parameters like hadronness, direction etc from both the reconstructions and apply the cuts we got from FLUTE to obtain the phasogram and hence the significance. We mix the parameter based on a certain weight k varying from 0 to 1 and $(1-k)$.

	hadronness	evt_number	run_number	srcposx_deg	srcposy_deg	dispx_deg	dispy_deg	mjd	millisec	nanosec	...	dirYDisp	ZdDisp	
0	0.318175	6953.0	5078762.0	0.010677	-0.397347	0.137708	-0.201474	58540.0	-10235856.0	574600.0	...	-0.174677	12.257343	-1:
1	0.673433	6956.0	5078762.0	0.010676	-0.397347	-0.061869	1.256779	58540.0	-10235854.0	888800.0	...	1.142949	13.515398	-1:
2	0.568281	6957.0	5078762.0	0.010675	-0.397347	0.350918	1.213819	58540.0	-10235853.0	790200.0	...	NaN	NaN	
3	0.932429	6958.0	5078762.0	0.010675	-0.397347	0.284686	0.663127	58540.0	-10235853.0	999400.0	...	-0.672108	11.701880	-1:
4	0.799583	6960.0	5078762.0	0.010674	-0.397348	1.200098	-0.432309	58540.0	-10235849.0	861000.0	...	NaN	NaN	
...
287371	0.794464	606342.0	5080152.0	-0.033331	-0.397867	0.675061	1.080989	58540.0	-9353083.0	991200.0	...	NaN	NaN	
287372	0.980635	606345.0	5080152.0	-0.033330	-0.397867	0.266482	-1.301565	58540.0	-9353081.0	510800.0	...	-1.313475	13.927994	-1:
287373	1.000000	606347.0	5080152.0	-0.033330	-0.397866	0.864832	-0.367123	58540.0	-9353074.0	584800.0	...	-0.978809	14.262596	-1:
287374	0.725738	606349.0	5080152.0	-0.033330	-0.397866	-0.219212	1.040501	58540.0	-9353072.0	501400.0	...	NaN	NaN	
287375	0.791476	606351.0	5080152.0	-0.033330	-0.397866	0.812755	1.029589	58540.0	-9353072.0	757600.0	...	-0.854346	14.392073	-1:

25289088 rows × 32 columns

Figure 3.4: Screenshot from Jupyter Notebook showing the RF Table

	event_id	obs_id	run_number	antistereoneess_noclean_call_good	src_pos_cam_x	src_pos_cam_y	pos_x_calihillas_clean_call_good	pos_y_calihill
0	55489.0	5080155.0	05080155	3.115378	0.001957	0.006948	0.318967	
1	55517.0	5080155.0	05080155	-2.308658	0.001957	0.006948	0.000273	
2	55521.0	5080155.0	05080155	6.165102	0.001957	0.006948	0.119820	
3	55569.0	5080155.0	05080155	2.425774	0.001957	0.006948	-0.003310	
4	55636.0	5080155.0	05080155	3.322217	0.001957	0.006947	0.157152	
...	
30523352	546564.0	5076461.0	05076461	1.083357	-0.005281	0.004845	-0.684246	
30523353	546565.0	5076461.0	05076461	3.388990	-0.005281	0.004845	-0.761665	
30523354	546570.0	5076461.0	05076461	-0.794306	-0.005281	0.004845	-0.207083	
30523355	546572.0	5076461.0	05076461	-0.024289	-0.005281	0.004845	-0.789017	
30523356	546576.0	5076461.0	05076461	1.114168	-0.005281	0.004845	-0.777666	

30523357 rows × 22 columns

Figure 3.5: Screenshot from Jupyter Notebook showing the CNN Table

Fig: The results obtained from two reconstruction method is used in tabular form in using pandas dataframe and are merged together for comparison.

1. Merge the event table of both CNN and RF using Run Id and Event Id as the key, which is in pandas dataframe. The tables are so big as it contains 25 millions event from RF table and 30 millions event from CNN table and hence to operate on it high CPU power computers at INFN Padova is used.
2. After merging, the parameters are mixed as shown below:

$$X_{mix} = k.X_{RF} + (1 - k).X_{CNN}$$

$$Y_{mix} = k.Y_{RF} + (1 - k).Y_{CNN}$$

\implies

$$\theta_{mix}^2 = (X_{mix} - X_{True})^2 + (Y_{mix} - Y_{True})^2$$

Here the X_{True} and Y_{True} are the true source position. Similarly we can also mix the hadronness and energy parameters like:

$$H_{mix} = K.H_{RF} + (1 - K).H_{CNN}$$

3. Now we will use the $\theta_{mix}^2, H_{mix}, E_{mix}$ and apply the cuts obtained on these parameters in our events from the flute part of RF analysis to obtain the phasogram. The number of on and off events we could calculate from our signal by analysing the phasogram obtained. As explained earlier, we will use the phase as shown in table below to obtain number of on and off events and hence obtaining the significance. Our aim is to see at what mixing the significance is high, and hence we plot the convex mixing to show significance vs K (our weight). The end part of this work is in progress, and we expect a good performance at certain level of mixing. In the figure 3.6 the comparison done for Markarian, the rise in significance is observed for all energy bins as we mix and then it again declined as we move towards fully random forest parameter. We expect similar behaviour from the Crab Pulsar, but with more concrete proof as the source dependent biasness is being resolved here.

Phase(ϕ)	
0.0 - 0.026	N_{on}
0.377-0.422	N_{on}
0.983-1.00	N_{on}
0.520 - 0.870	N_{off}

3.4 Expected Plots

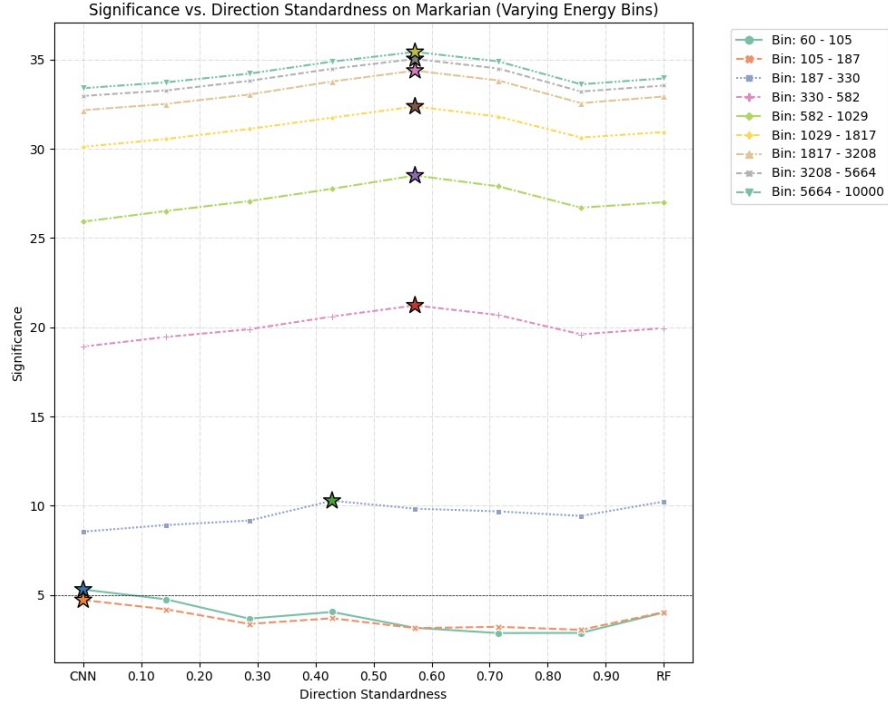


Figure 3.6: Significance vs Weight Plot obtained for Markarian

Fig: The image here shown is obtained by mixing the direction parameters from two reconstruction method and significance is calculated using cuts from θ_{mix}^2 . We expect to obtain similar behaviour, and expect to get better significance at certain mixing k when same result is produced using Crab Pulsar. The point to be noted here is that at k=0, we will observe fully CNN significance and at k=1, we will observe only RF significance.

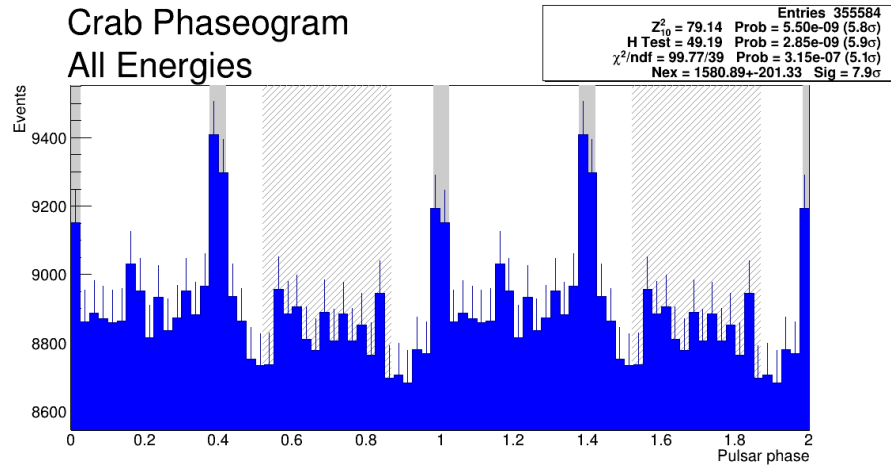


Figure 3.7: Phaseogram obtained using RF analysis, for 20 hours of data used for comparison with significance of 7.9σ

We expect to obtain a better phaseogram than above, when we plot at maximum significance after mixing the parameters from both CNN and RF for Crab Pulsar. The work with Crab Pulsar is in progress as we have encountered some errors in array of data, which we hopefully will solve soon.

Chapter 4

Fermi-Lat Analysis

Fermi is a space-based telescope that directly detects photons. However, the energy range up to which it could detect is less than that of MAGIC i.e it operates in the range of 20MeV - 300 GeV and has an effective area of $1m^2$. Unlike the MAGIC, the fermi data and its tools are open to the public. In the coming section, the data of 2011 is analyzed using two methods i.e. Aperture Photometry and Unbinned Likelihood Analysis.

4.1 Aperture Photometry

Aperture Photometry is the easier, less time taking method to analyze the data and obtain the curves like that of the light curves. However, its sensitivity and accuracy is less. In the fermi analysis, the data is obtained assuming the source of our interest in the center and corresponding that we have the region of interest around the source whose data we have extracted. In the first step we choose the event in which we are interested by performing cuts using the gselect tool. To have good data gtmktime tool is used. It uses the field of view of the telescope to that of the event angle with respect to the aperture and zenith. Gtbin is then used to do the binning in time to obtain the light curve followed by gtxposure to calculate the exposure(cm^2s^{-1}).

With this, the light curve is calculated. Below is the light curve obtained by this method with the error bar for the Crab Pulsar of 2011.

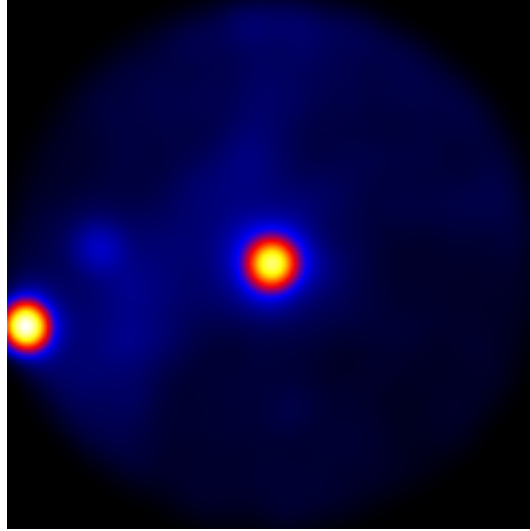


Figure 4.1: Counts Map for the source showing Crab Pulsar at the center

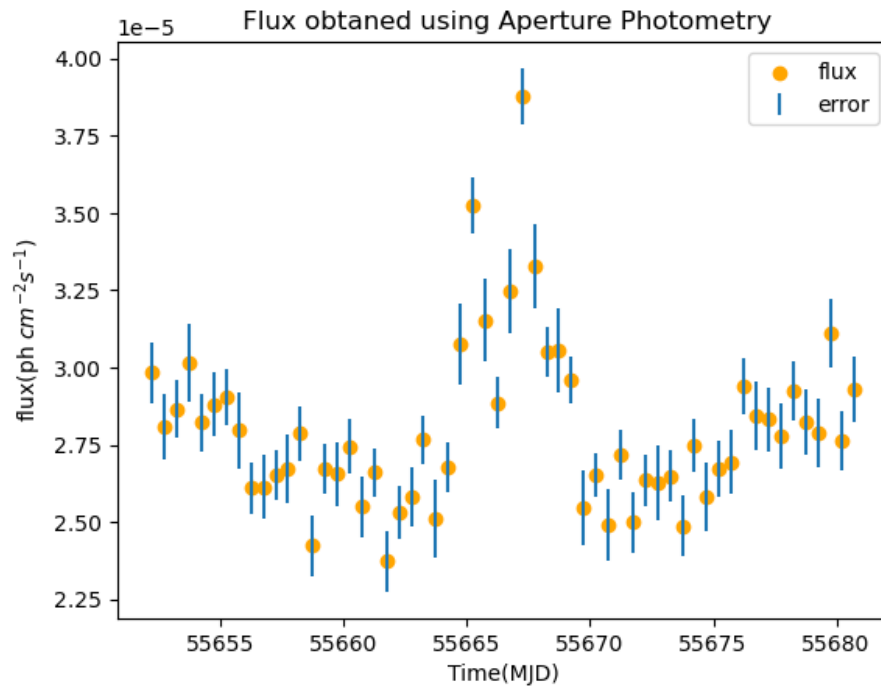


Figure 4.2: Light curve Plotted using Aperture Photometry for April 2011

However, since in this method, the sensitivity is not good, and the background is

not modeled hence the observed flux is always greater than the actual. Therefore we move to the unbinned likelihood analysis which is more accurate as compared to the aperture Photometry.

4.2 Unbinned Likelihood Analysis

Likelihood: The likelihood is the probability of obtaining the given data given by our model. In this method, we assume some model of our source, and a model of the model background. It finds the best parameter which we have used in our model that gives a high probability of obtaining our data.

Steps: Just like above the initial part i.e gtsselect and gtmktime is the same here also. However here the exposure maps are calculated differently. First, the livetime cube is calculated.

Live Time Cube: The response function fermi Lat detector depends on the angle between the source and the detector normal. Therefore the no. of photons detected by the fermilat would depend on the amount of time the detector is observing source at different angles. The livetime cubes are defined on the Healpix grid on the sky and inclination angle in bins since it cant be generated for the continuous one.

Exposure Map: This tool calculates the predicted number of photons in the given region of interest for the source in our model. The source model should contain the area of interest i.e source region more than the region of interest and all the point sources should be included in our model. The gtpexp needed to calculate the exposure also needs the livetime cube generated by gltcube.

Modelling the source: Once this is done we need to model the source with varying parameters. For the crab Nebula which is a point source, the power law behavior is assumed i.e:

$$\frac{dN}{dE} = N_o \left(\frac{E}{E_o} \right)^\gamma$$

where the prefactor N_o , index γ , and the scale E_o is left as free parameter. The background is also modeled for galactic emission and this also includes cosmic ray background. Its parameter could be downloaded from the fermi website, and this is fixed.

once this is done diffuse response from the background and the source is calculated which depends on the instrument response function.

gtlike: To perform the analysis step i.e model fitting and get the fluxes in the given time bin, gtlike is used.

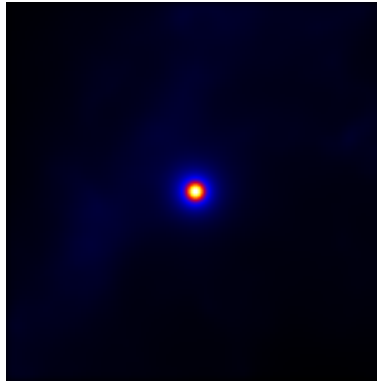


Figure 4.3: Source model got using Unbinned Likelihood Analysis

4.3 Result and comparison

While analyzing the data of 2011, using unbinned likelihood analysis by doing weekly binning flare has been observed in a certain time. To analyze it properly, the light curve of 2011 April is produced by doing 12-hour binning in which the flare could be observed clearly.

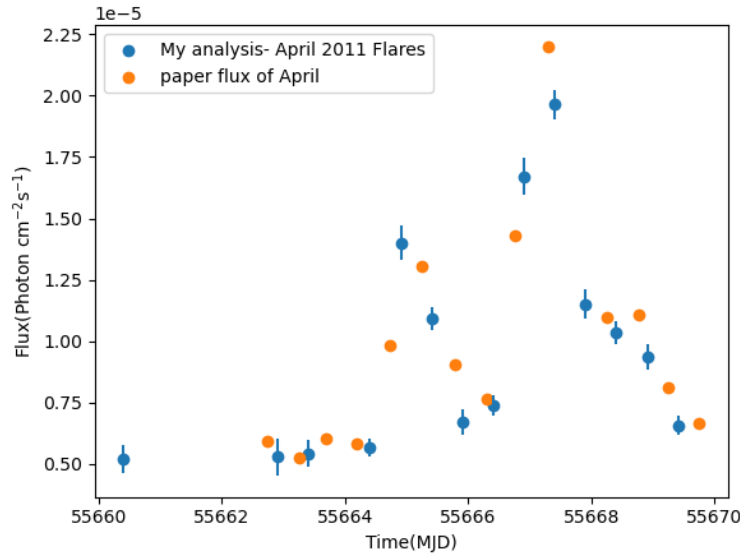


Figure 4.4: Comparison of analysis with Striani et al. [12]

This analysis has also been done by [12] hence to compare our analysis with theirs the plot is shown in the figure 4.4 which seems to overlap. This kind of behavior has also been observed by AGILE in the oct 2007 and also in 2012. The reason for this kind of behavior or sudden rise in flux or the flare is given as the magnetic reconnection which leads to very high sudden acceleration of particles present there. However, this solution is still under debate and proper analysis is needed to be done. For the next part, we will be going to analyze years 2010-2018 of Fermi-lat data.

4.4 Light Curve Analysis(2010-2018)

Through the unbinned Likelihood Analysis, I obtained the light Curve Plot for the year 2010-2018 for the Crab Pulsar. The flare like behaviour which has been observed early in the year 2011 and 2007 was seen recurring along the analysis period. In order to identify flares in the flux varying plot, first of all I obtained the log-log histogram plot for the flux. Then it is fitted with the gaussian Curve as indicated in the figure. Since we are expecting the flares to not to occur too often, hence we mark the points

above $\mu + 3\sigma$ as the flaring points, as they will account for less than 1% of the flux.

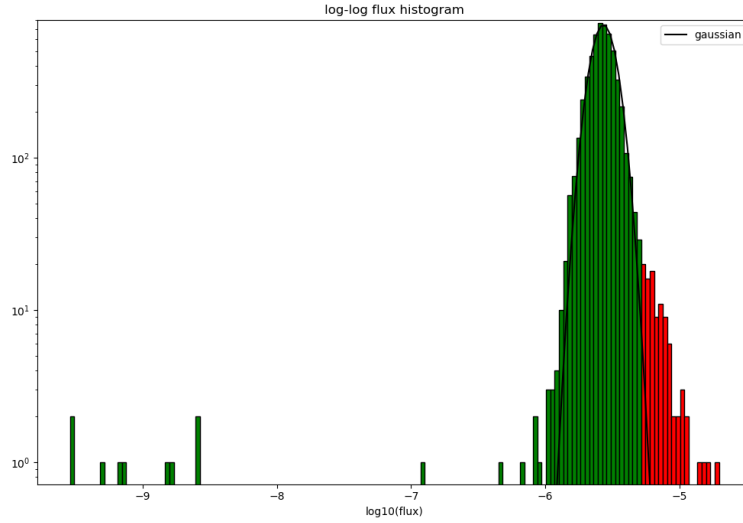


Figure 4.5: log log histogram plot of flux obtained from Analysis and identification of flares. The flaring points belong to red marked histogram which lie above $\mu+3\sigma$.

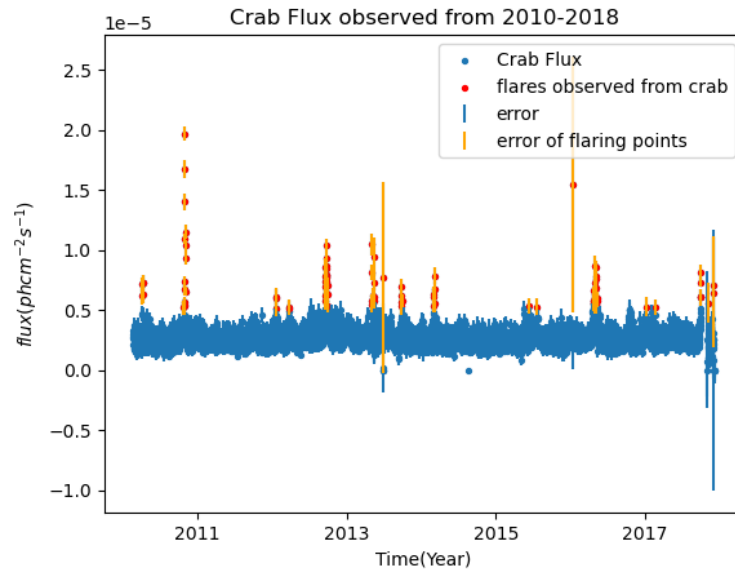


Figure 4.6: Light Curve obtained for the year 2010-2018 for Crab Pulsar using the Likelihood Analysis Method and the flares observed.

The table shown here shows the mean time in MJD of the flares and the duration for which they were observed :

Mean Flaring Point (MJD)	Duration(Hours) 12hrs x No. of flaring points observed
55459.90	12 x 5
55665.905	12 x 5
56111.90	12 x 3
56173.90	12 x 2
56358.22	12 x 20
56582.58	12 x 6
56595.00	12 x 4
56635.25	12 x 1
56725.50	12 x 4
56886.41	12 x 6
57349.75	12 x 1
57388.25	12 x 1
57565.75	12 x 1
57673.85	12 x 26
57924.75	12 x 1
57971.75	12 x 1
58190.05	12 x 5
58227.75	12 x 1
58254.25	12 x 2

To understand whether the flaring episode I observed is random, I obtained the histogram plot of time delay, i.e., the time difference between two consecutive flaring episodes. The histogram representation is found to be exponentially distributed, and the deviation was not that significant. This is evident from figure 4.7; in fig 4.7, the histogram representation of time delay is plotted in log scale, and hence the correspondent fit would be linear, which is lying within the error range. Hence with these low statistics of flaring episodes, we can conclude that the process is compatible with the random process and the flaring episodes are independent of each other.

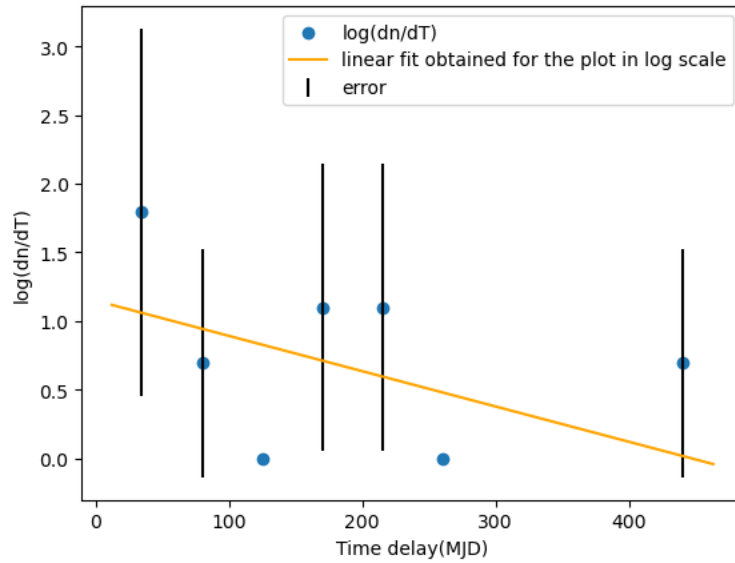


Figure 4.7: Plot of the counts of time delay in log scale

Chapter 5

CONCLUSIONS

In this thesis, my research focused on studying the emission of very high-energy gamma rays from the Crab Pulsar and Nebula. I conducted an analysis of both the Crab Pulsar and Nebula using the MAGIC Telescope and the Fermi-Lat Telescope. The main part of my thesis centered around the MAGIC Analysis, specifically comparing the reconstruction methods of Convolutional Neural Network (CNN) and Random Forest (RF).

Chapter I primarily delved into the theoretical aspects of very high-energy (VHE) emission and the properties of atmospheric showers, which enable us to capture and visualize the emission and gain insights into its source.

Using the MAGIC telescope, I analyzed the data for the Crab Nebula and obtained the flux variability, represented by the light curve, as well as the spectral energy distribution $E^2 \frac{d\phi}{dE}$.

By employing the Sum Trigger in MAGIC, we were able to observe gamma ray events occurring at lower energies, specifically below 100 GeV. Analyzing the data obtained through the sum trigger, I successfully detected the signal from the Crab Pulsar that was not observable using the standard trigger. It is worth noting that the θ^2 obtained

for the Crab Nebula and Pulsar differed, as the Crab Nebula acted as background for the Crab Pulsar. Furthermore, I derived the phasogram, which exhibited a significance of 5.1σ .

As time progresses, it becomes crucial to enhance existing analysis methods and detect sources with greater significance. I conducted a comparative study between the RF and CNN methods of reconstruction for energy, direction, and the probability of separating gamma and hadron particles. The CNN reconstruction method, developed by [11], is expected to achieve superior performance since it employs the calibrated image as input, reducing information loss during image cleaning. For the comparison, I utilized the Crab Pulsar and aimed to determine the significance at different weightings while combining the parameters. This is of utmost importance as it resolves the bias associated with source-dependent CNN reconstruction by focusing on the phase analysis. Although this work is still in progress, we anticipate that at a certain combination of weights, the performance will surpass both RF and CNN methods.

In the final part of my thesis, I analyzed the Crab Pulsar using Fermi-Lat data spanning from 2010 to 2018. I employed the unbinned likelihood analysis method and observed recurring flares in the light curve during this period. From the exponential distribution of the flares with no significant deviation, I concluded that they are occurring randomly in time that is independent of each other.

Bibliography

- [1] Patrizia A Caraveo. Gamma-ray pulsar revolution. *Annual Review of Astronomy and Astrophysics*, 52:211–250, 2014.
- [2] Robert M Wagner. *Measurement of VHE γ -ray emission from four blazars using the MAGIC telescope and a comparative blazar study*. PhD thesis, PhD thesis, Technische Universitaet Muenchen, 2006.
- [3] Rubén López Coto. *Very-high-energy gamma-ray observations of pulsar wind nebulae and cataclysmic variable stars with MAGIC and development of trigger systems for IACTs*. Springer, 2016.
- [4] Riccardo Paoletti, R Cecchi, D Corti, F Dazzi, M Mariotti, R Pegna, and N Turini. The trigger system of the magic telescope. *IEEE transactions on nuclear science*, 54(2):404–409, 2007.
- [5] Dazzi F. *Phd Thesis*. Udine(Italy), 2012.
- [6] Jezabel R García, F Dazzi, D Häfner, D Herranz, M López, M Mariotti, R Mirzoyan, D Nakajima, T Schweizer, and M Teshima. Status of the new sum-trigger system for the magic telescopes. *arXiv preprint arXiv:1404.4219*, 2014.
- [7] Alessia Spolon. *Phd Thesis*. Univerista’ degli studi di Padova, 2022.
- [8] A Michael Hillas. Cerenkov light images of eas produced by primary gamma. In *19th Intern. Cosmic Ray Conf-Vol. 3*, number OG-9.5-3, 1985.

- [9] T-P Li and Y-Q Ma. Analysis methods for results in gamma-ray astronomy. *Astrophysical Journal, Part 1 (ISSN 0004-637X)*, vol. 272, Sept. 1, 1983, p. 317-324., 272:317–324, 1983.
- [10] Pietro Grespan. *Master Thesis*. Univerista' degli studi di Padova, 2020.
- [11] Ettore Mariotti. *Master Thesis*. Univerista' degli studi di Padova, 2019.
- [12] E Striani, M Tavani, V Vittorini, I Donnarumma, A Giuliani, G Pucella, A Argan, A Bulgarelli, S Colafrancesco, M Cardillo, et al. Variable gamma-ray emission from the crab nebula: Short flares and long “waves”. *The Astrophysical Journal*, 765(1):52, 2013.